2.5D Micromachined 240 GHz Cavity-Backed Coplanar Waveguide to Rectangular Waveguide Transition

Mehrnoosh Vahidpour, *Student Member, IEEE*, and Kamal Sarabandi, *Fellow, IEEE*

***Abstract*—A novel cavity-backed coplanar waveguide (CBCPW) to rectangular waveguide transition having a 2.5D geometry compatible with micromachining fabrication technique is presented. This transition makes use of a short-circuited pin (as opposed to a suspended probe) in conjunction with resonant sections of CPW line over the broad wall of a reduced height waveguide segment to facilitate impedance matching. Although the bandwidth of this transition is smaller than the standard suspended probe transitions, its fabrication at submillimeter-wave and terahertz bands is rather straightforward and does not require assembly of many small parts with very high precision. The design procedure starts from an equivalent circuit model which is then fine-tuned using a full-wave approach. A silicon micromachining process for the fabrication of the proposed transition is presented. To validate the design and demonstrate the feasibility of the fabrication process, a prototype transition operating at 240 GHz is fabricated and tested. It is shown that a back-to-back transition prototype at 240 GHz provides less than 1 dB of insertion loss over more that 17% fractional bandwidth. It is also shown that the measured S-parameters of the back-to-back transition are in good agreement with the simulation results. The microfabrication process and associated tolerances allows for scaling the dimensions and frequency of operation to THz frequencies.**

***Index Terms*—Cavity-backed CPW, E-plane probe excitation, micromachining techniques, waveguide transition.**

I. Introduction

IN RECENT years, the submillimeter-wave (SMMW) and terahertz (THz) frequency spectrum of electromagnetic waves have received significant attention due to their applications in wideband secure communication, environmental and biomedical sensors, as well as miniaturized radar-based navigation and imaging systems [1]. Since the wavelength in this band is rather small, compact and fully integrated circuits on a single chip or wafer can be realized. For such circuits, devices and components compatible with planar and 2.5D structures are of interest. Losses in planar transmission lines at millimeter-wave frequencies and above can impair the performance of integrated antenna arrays with corporate feed structures or the performance of filters (insertion loss and frequency selectivity) realized on such transmission lines. As an alternative, often times rectangular waveguides are utilized for the antenna feed and filter designs to avoid the high Ohmic and dielectric losses of planar transmission lines.

Active components and devices such as amplifiers, mixers, and multipliers are most conveniently fabricated and integrated on planar transmission lines. To connect such devices to antennas, appropriate transitions from these transmission lines to waveguides are needed. At high MMW and low THz frequencies, waveguide structures can be directly fabricated on silicon or glass wafers using micromachining methods allowing for fully integrated system to be fabricated on a single wafer. Micromachining is also a preferable approach at these frequencies as it offers the required fabrication tolerances and can eliminate the need for assembling different parts and components. Various microstrip or coplanar waveguide-(CPW) to-rectangular waveguide transitions have been proposed in the past ([2]–[14]) at X- and Ka-bands, fabricated using standard machining techniques. Many of these techniques, however, cannot be adopted for micromachining as they require multiple parts with complex 3D geometries and/or different dielectric materials in their construction. The literature concerning microfabrication of waveguide structures at W-band and higher is rather sparse. There have been several attempts to fabricate W-band waveguides with low-cost microfabrication techniques such as lithography [15]–[17]. However, in these techniques, the height of the waveguide is limited by the maximum thickness of the spun photoresist, limiting the fabrication to reduced-height waveguides, which suffer from high attenuation. Taking advantage of the "snap-together" technique [16], a rectangular waveguide was fabricated in two halves and then the halves were put together to form a complete waveguide. An alternate technique for etching the waveguide is deep reactive ion etching (DRIE) of silicon which is a viable approach for fabrication of high-performance micromachined waveguide structures. In [18] and [19], transitions using microfabrication processes, but with separately fabricated and assembled probes, have been reported for both diamond and rectangular waveguides showing 20% bandwidth. Another high-precision silicon micromachined transition with the capability to integrate filters has been proposed in [20] and [21] and shows wideband characteristics at the same frequency range. However, these transitions involve a high degree of fabrication complexity, complex three-dimensional geometries, assemblies of various parts, and a high number of steps needed for construction which cannot be easily implemented in MMW and sub-MMW frequency bands.

Manuscript received November 22, 2011; revised February 02, 2012 and March 01, 2012; accepted March 09, 2012. Date of publication May 02, 2012; date of current version May 08, 2012. This work was supported by the U.S. Army Research Laboratory under Contract W911NF and prepared through collaborative participation in the Microelectronics Center of Micro Autonomous Systems and Technology (MAST) Collaborative Technology Alliance (CTA).

The authors are with the University of Michigan, Department of Electrical Engineering and Computer Science, Ann Arbor, MI 48109 USA.

Color versions of one or more of the figures in this paper are available online at http://ieeexplore.ieee.org.

Digital Object Identifier 10.1109/TTHZ.2012.2191150

In this study, we propose an in-plane transition from cavity-backed CPW (CBCPW) line to rectangular waveguides compatible with silicon microfabrication techniques that does not require assembly of multiple parts. In this approach, the need for fabricating a suspended resonant probe is eliminated and an effective wideband transition is achieved using two different resonant structures, namely, shorted CPW line over the broad wall of the waveguide followed by an E-plane step discontinuity. A prototype of this transition at Ka-band has been previously fabricated using standard machining methods and measured to validate its performance [22]. The structure is designed to be very simple with all its features aligned with the Cartesian coordinate planes in order to make it compatible with microfabrication processes. The transition is modeled by an equivalent circuit to help with the initial design which is then optimized using a full-wave analysis. A back-to-back structure for standard WR-3 rectangular waveguides is microfabricated on two silicon wafers which are bonded together using gold–gold thermocompression bonding technique (a hermetic bond) to ensure the excellent metallic contact needed for the formation of the waveguide. The validity of the transition design is demonstrated by measuring the S-parameters of a 240 GHz back-to-back transition prototype using a vector network analyzer with frequency extenders connected to WR-3 GSG probes [23]. The measured results show a very good agreement with the simulations.

II. Micromachining Design Constraints

Traditional CPW to rectangular waveguide transitions based on E-plane probe excitation involve attaching a suspended resonant probe to the center conductor of a CPW line going through the broad wall of the waveguide [10], [11], as shown in Fig. 1(a). This transition covers the waveguide band and can easily be fabricated at microwave and low MMW frequency bands using the standard fabrication and assembly methods. At high MMW and THz frequencies where the tolerance of standard machining methods are not sufficient, micromachining techniques can be used. Although micromachining can provide the required tolerances for fabrication of small and high precision devices, there are many limitations on what can be fabricated. For example structures that are 2.5D (prismatic structures) are simple to fabricate. Also structures formed by stacking wafers with 2.5D geometries are possible. However microfabrication of a very small suspended probe within a hollow waveguide patterned in a silicon wafer is rather challenging. In [20] and [21], using non-contact lithography, the CPW line is patterned after etching the suspended probe. However, the process of spinning photoresist uniformly in the presence of the probe is very challenging. Alternatively, if the CPW is patterned first, the surface cannot be etched afterward to construct the probe and also attaching a suspended probe to wafer in the final step is not practical due to its small dimensions.

The microfabrication of a transition can be performed conveniently using two stacked wafers, if a short-circuited probe extending the entire height of the waveguide is used. The waveguide trench and the probe are patterned and etched on one substrate while the CPW line is patterned on another substrate, as shown in Fig. 1(b), which are eventually bonded together. Nonetheless, a short-circuited probe acts purely reactive and

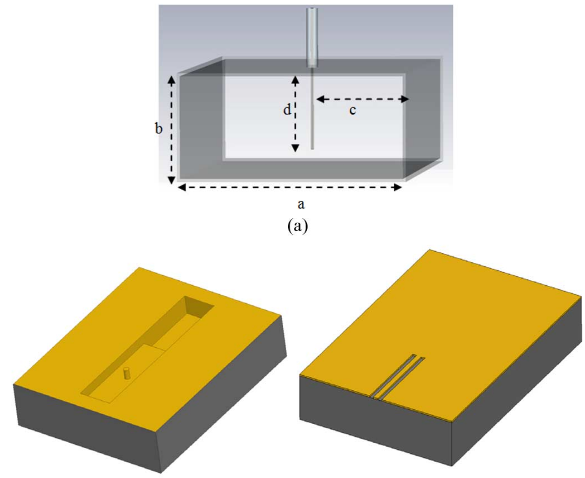

(a)

(b)

Fig. 1. (a) Suspended E-plane probe excitation. (b) Microfabrication of short-circuited probe for in-plane CPW is performed on two wafers: one for waveguide trench and the probe, the other for CPW line. The two wafers are bonded to form the transition.

cannot be matched to the CPW line. To properly excite a waveguide with this probe, a resonant condition must be achieved to eliminate the probe reactance. It is well known that a pin terminated by the broad wall of a rectangular waveguide acts as an inductive element whose inductance is inversely proportional to its diameter and the waveguide dimensions [24]–[27]. To compensate for the inductance of the shorting pin X_p, a capacitive element is needed. Since a step discontinuity in the E-plane of the waveguide acts as a capacitive element, it can be used to compensate for the inductive behavior of the pin. That is, a resonant condition can be realized by terminating a short-circuited pin in a reduced-height waveguide with a step transition from the reduced-height waveguide to the standard-size waveguide. The length of the waveguide between the pin and the step transition can be used to control the capacitance seen by the inductance. Also, the waveguide height can be used to control the capacitance at the step transition point.

III. Transition Designs

A. Cavity-Backed CPW to Rectangular Waveguide Transition

CBCPW lines are preferred at very high frequencies for mounting active components due to their low-loss characteristics. Hence, a transition from a novel low-loss membrane supported CBCPW (see [28, Fig. 2]) to rectangular waveguide is considered here. In CBCPW structure the dielectric substrate is removed and the line is suspended over a hollow trench in order to eliminate the dielectric loss. For fabrication purposes, a dielectric membrane on top of the line supports the suspended line over the trench. This line can be easily incorporated with hollow rectangular waveguides [28].

The proposed transition is presented in Fig. 2(a). Unlike the previously microfabricated transitions, the CBCPW line is positioned in-plane with the waveguide top wall and can be easily fabricated using two stacked silicon wafers. The CPW line printed over the top waveguide wall is given different characteristic impedance in order to create a transmission line resonator including the pin. This second resonator that

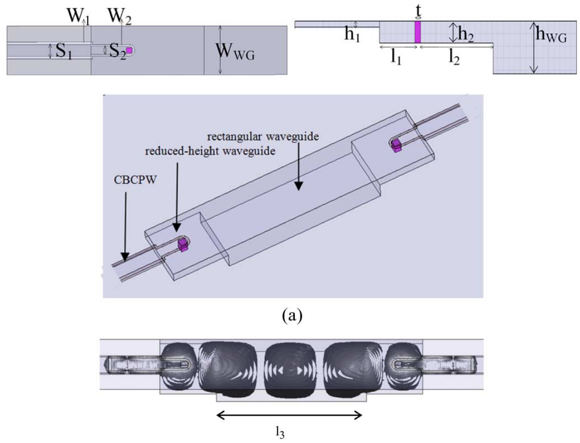

Fig. 2. (a) CBCPW to rectangular waveguide transition, top view, side view and the perspective of a back-to-back configuration which includes a transition from CBCPW to CPW, CPW to reduced-height waveguide and reduced-height waveguide to the standard WR-3 rectangular waveguide. (b) Simulated electric field distribution inside the structure.

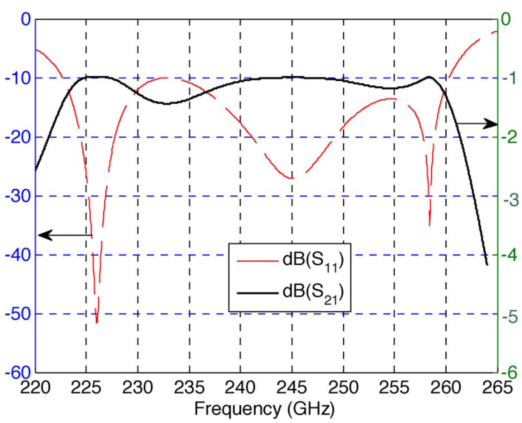

Fig. 3. Transmission and reflection coefficient of the back-to-back structure for $S_1 = 210\ \mu$m, $g_1 = 45\ \mu$m, $S_2 = 140\ \mu$m, $g_2 = 30\ \mu$m, $h_1 = 46\ \mu$m, $l_1 = 330\ \mu$m, $l_2 = 450\ \mu$m, $t = 100\ \mu$m, $h_2 = 143\ \mu$m, $W_{\rm WG} = 864\ \mu$m, $h_{\rm WG} = 432\ \mu$m $l_3 = 5.24\ \mu$m, showing 17% bandwidth and insertion loss of lower than 1.5 dB for the back-to-back structure.

is coupled to the pin and step resonator inside the waveguide provides another impedance match. The center conductor of the CPW line is open-circuited at the location of the pin and the pin is connected to the lower wall of a reduced-height waveguide. On the other side of the pin, the reduced-height waveguide is short-circuited at a distance to appear as another reactance parallel to the pin inductance.

To design the transition, first the dimensions of waveguide and CBCPW line are chosen based on the desired frequency range. The initial values of elements of the circuit model are selected using the analytical formulas and measurement results reported in [24] and [25]. These values along with the length of waveguide and CPW line sections are optimized using transmission line analysis of the circuit model to obtain the resonant behavior. A structure based on these values is designed and then optimized a using full-wave simulator (Ansoft HFSS) [29], [30].

The electric field distribution and the reflection coefficient of the optimized structure are represented in Figs. 2(b) and 3 for the back-to-back transition. It is shown that transition with a transmission coefficient better than -1.5 dB over 17% fractional bandwidth can be achieved.

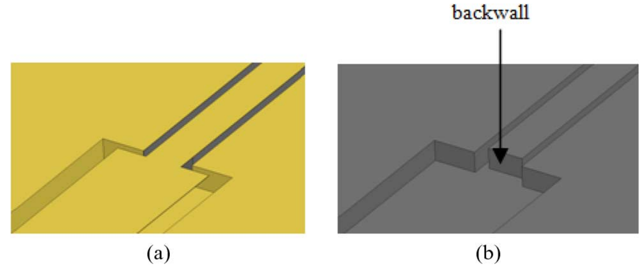

Fig. 4. (a) Schematic of the transition from grooved CPW to the CBCPW (b) Bottom substrate with top layer removed. The backwall shown in (b) should not be covered with gold.

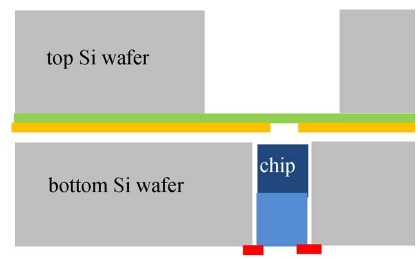

Fig. 5. Schematic of the thru-wafer transition for active component integration.

B. Grooved CPW to CBCPW Transition

The low-loss CBCPW line [28] is suspended on a membrane and hence, measurement probes cannot be placed on it since even a small amount of pressure applied by the probes might break the membrane. On the other hand, conventional CPW has dielectric substrate and is stiff enough for the probes pressure which makes it more convenient to use for measurement purposes. Hence a transition from a conventional CPW to CBCPW is required to characterize the performance of a back-to-back transition. The proposed structure is shown in Fig. 4. For the ease of fabrication and lower loss, a grooved CPW is designed. The substrate is made of silicon and loss tangent is calculated based on the resistivity of silicon wafer. It should be noted that the response of this transition is eventually de-embedded from the final measured results.

The final fabricated structure is a back-to-back configuration from grooved CPW to CBCPW to reduced height waveguide to standard-height waveguide.

C. Integration of Active Components

Although the main objective of this paper is to present the design and fabrication of CBCPW to waveguide transition, it is also useful to discuss the approach for integrating non-silicon-based active devices in such transitions. This can be done from the topside using capacitively-coupled flip chip method. At high MMW and sub-MMW frequencies allowing small overlap areas (as small as 250 μm $\times$ 750 μm) of metallic traces of CPW lines on the chip and the transition with air-gaps as high as 5 μm are sufficient for very good electric coupling between the chip with active components and the CBCPW line. To simplify the alignment issues a hole in the bottom wafer with approximate dimensions of the chip created through which the chip can be guided and come in contact with the metallic traces of the transition CPW lines as shown in Fig. 5.

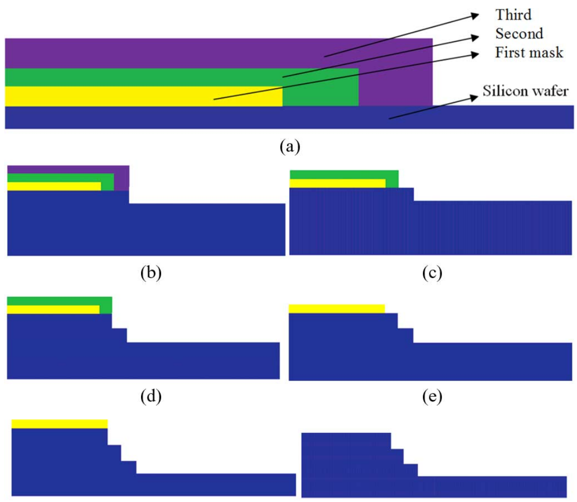

Fig. 6. Multi-step etching process for the bottom wafer. (a) Three different mask layers are deposited and patterned. (b) Wafer is etched with the last mask layer down to the desired thickness. (c) Mask layer is removed. (d) Wafer is etched with the next mask layer. (e) Mask layer is removed. (f) Wafer is etched with the final mask layer. (g) Mask layer is removed. The process can be carried on for more number of steps as long as the appropriate mask layer is chosen.

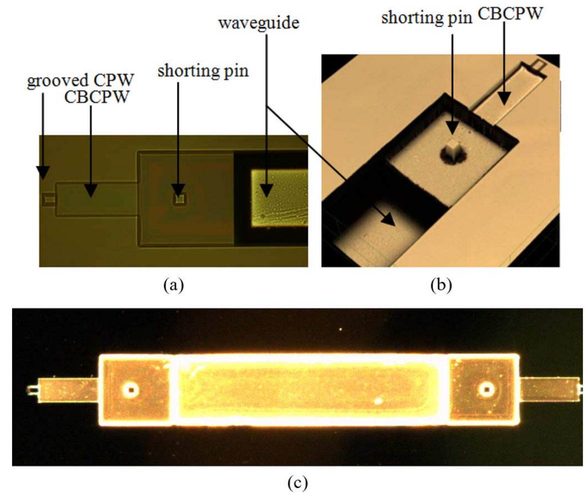

Fig. 7. Microscopic image of the three-step etching (a) before etching with LPCVD, PECVD silicon oxide and photoresist mask layers (b) after etching (depth measurement using 3D optical surface profiler). (c) Back-to-back structure. Etching with these mask layers results in highly smooth etched areas with less than 100 A roughness.

IV. Microfabrication Process

The fabrication of the transition structure is performed on two silicon wafers which henceforth will be referred to as bottom and top wafers. The bottom wafer includes the multi-step structure, the short-circuited pin and, the CBCPW and CPW grooves. The top wafer includes the membrane and the gold patterns of CBCPW and CPW. These gold-coated wafers are ultimately attached using gold thermocompression bonding technique.

A. Bottom Wafer

A multi-stage approach for etching silicon wafer using DRIE method is developed to fabricate the stepped structure of CBCPW and waveguide. Unlike wet etchants which etch silicon anisotropically along the crystal planes, DRIE is used to create deep, steep-sided holes and trenches in wafers. This approach allows creation of trenches and groove with aspect ratios as high 20:1 or more.

To create a multi-step structure on a silicon wafer, multi-step masking, pattering, and etching will be required. In this process, the wafer is patterned successively with different mask materials. Then it is etched with the last mask to the desired depth, the mask is removed and etching is continued with the next mask to the desired depth for the next step. This process can be carried on to achieve different steps of different depth within the silicon wafer. The fabrication process is illustrated in Fig. 6. By carefully managing etching time and thickness of the mask layers, a consistent process can be achieved. Fig. 7(a) and (b) shows the microscopic image of the fabricated three-step structure before and after etching on low-resistivity silicon wafers (0–100 $\Omega \cdot$ cm). Fig. 7(c) shows the image of the fabricated back-to back structure.

One difficulty in the fabrication of the grooved CPW and the CBCPW on the same wafer pertains to the fact that the bottom wafer on which the cavity of CBCPW and the grooved CPW are to be fabricated must be metalized by gold, however, the grooves of the CPW cannot be metalized or otherwise the CPW will be short-circuited. Also, the backwall of the grooved CPW shown in Fig. 8(b) should not be gold-coated. In order to protect these areas from gold deposition, patterning is found to be practically impossible as was initially envisioned. To overcome this problem, we developed a technique utilizing the fact that gold deposition is not possible within very narrow grooves with very high aspect ratios. We have experimentally shown that when the width of a trench is less than 5 μm and the aspect ratio is higher than 10, gold is not deposited on the bottom and lower portion of the side walls of the trench. To fabricate the structure of Fig. 8(b) without groove metallization, the geometry shown in Fig. 8(a) is proposed. In this structure, the thin protecting walls shadow gold deposition because of the high aspect ratio of the channels. The walls will be eventually removed by dry silicon etching.

After the wafer is etched, a layer of silicon oxide is deposited as a diffusion barrier before gold-coating the surface. This layer is needed for gold bonding to stop diffusion of silicon through the gold layer during bonding. Then titanium or a combination of chrome and titanium with thicknesses of 300 $\sim$ 500 Å is deposited as the gold adhesion layer. Due to around 50% step coverage, gold thickness of 1 $\sim$ 1.5 μm is needed in order to ensure at least 0.5 $\sim$ 1 μm of gold is deposited on the sidewalls. At the final step, the thin shadow walls in the CPW grooves are removed using an isotropic silicon etchant. The etch time depends on the gap width between the walls and is longer for thinner and deeper gaps as it is hard for the gas to penetrate inside these areas. However, in order to reduce damage to other areas, the wafer was exposed to the etchant over a relatively short period of time to make the walls frail. Ultrasonic vibration is then used to remove the fragile walls completely as shown in Fig. 8(b). It is observed that the walls are completely removed after 5 min of exposure to XeF_2 and 2 minutes of ultrasonic vibration. Fig. 8(c) shows the SEM image of the end wall of the grooved CPW (tilted 20° for a better view of the backwall) which verifies that the shadow walls prevented gold deposition over the vertical walls of the middle silicon block.

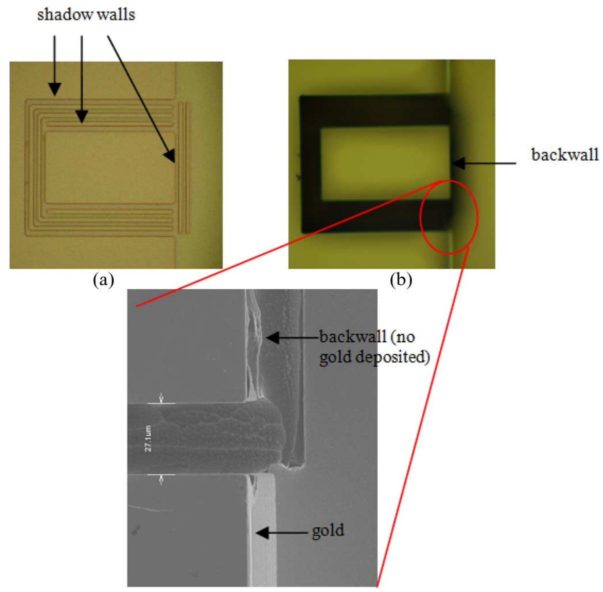

Fig. 8. Grooved CPW (a) before and (b) after removing the shadow walls. (c) SEM photo of the backwall (tilted 20°) which verifies that the shadow walls prevented gold deposition effectively.

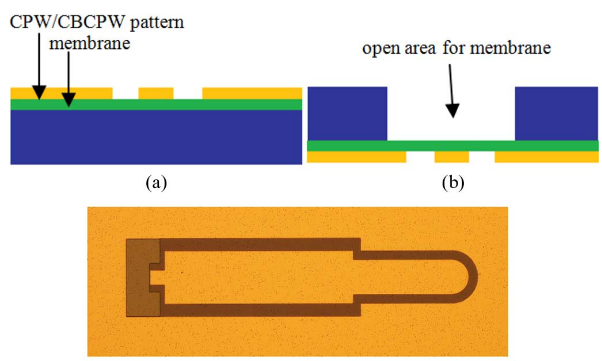

Fig. 9. Top wafer fabrication process. (a) a stacked layer of LPCVD $SiO_2/Si_3N_4/SiO_2$ as a membrane covered by a layer of gold. Then the gold is patterned with the mask of the grooved CPW and CBCPW lines. (b) The wafer is flipped over and the backside is removed from the top of the areas where line is suspended. (c) Fabricated CPW/CBCPW on the top wafer.

B. Top Wafer

A second wafer is used to cover the top part of the waveguide structure. On this wafer, first a stacked layer of LPCVD $SiO_2/Si_3N_4/SiO_2$ membrane is deposited. This three-layer membrane is chosen to minimize stress so that the membrane does not buckle after the top silicon is removed. At the next step, the wafer is coated with gold which is patterned and etched with the mask of the grooved CPW, CBCPW and narrowed CBCPW lines. In order to suspend the center conductor of CBCPW on the membrane, backside of the wafer is etched on the areas around the CBCPW line. Fig. 9(a) and (b) shows the fabrication process of the top wafer and Fig. 9(c) represents the fabricated top wafer.

C. Bonding

As the final step, the top and bottom wafers are bonded using gold-to-gold thermocompression bonding process following the procedure presented in [31] and [32]. The bonding requires a high-force on a surface with a high temperature; around 400 °C but much lower than gold melting point. Before bonding, the wafers must be aligned carefully. Since in certain areas over the top wafer silicon is removed and the membrane is transparent, the bottom wafer can be seen easily and markers can be used for precise alignment. This method provides much higher precision bond-aligning compared to the backside alignment technique.

After aligning and clamping the wafers together, they are placed inside the bonding chamber, and a pressure of 4000 torr and temperature of 375 °C is applied [32] for 40 min. Fig. 10 shows the top view of the structure after bonding. It is observed that the quality of gold does not degrade after bonding due to the utilization of a high quality diffusion barrier layer. Fig. 10(b) shows the full view of the final structure and a large open area where the back side of the center conductors of the grooved CPW lines are observable. This open area allows easy placement of the GSG probes. The bond-alignment error is maintained below 5 μm among different samples.

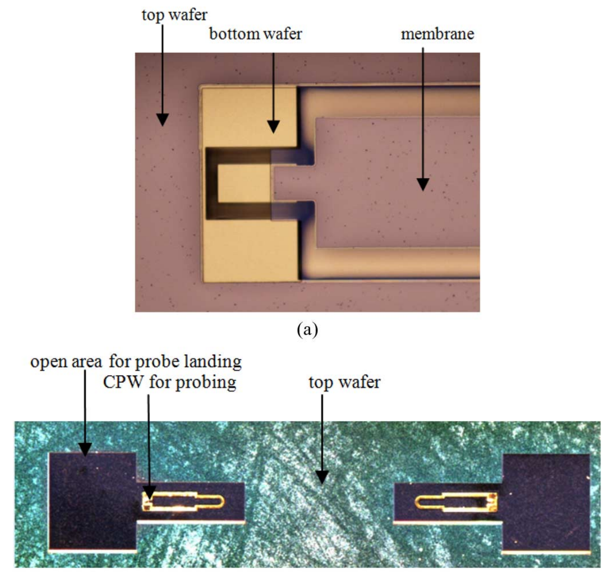

Fig. 10. Final fabricated transition. (a) CPW-CBCPW bottom and top wafers are aligned well and bonded together. The quality of gold does not degrade after bonding (b) top view of the transition. The areas on the backside of the lines are also etched to facilitate landing of the probe on the substrate.

V. Sensitivity Analysis

Despite high level of accuracy, micromachining with multiple fabrication processes as shown above is prone to errors caused by small misalignments, as well as geometrical distortions resulted from lithography and DRIE etching. Etching silicon very deep ($\sim$ 432 μm) with uniformity and high precision over large areas is rather difficult. The etch rate in the DRIE chamber might vary depending on the temperature, the position of the feature on the wafer, RIE lag effect, etc. As a result, it is most likely that the required etch depth values are not very precise. Hence it is essential to examine the sensitivity of the structure to the fabrication tolerances. For the nominal values of the WR3 and reduced height waveguide depths ($h_{\mathrm{WG}} = 432$ μm and $h_2 = 159$ μm, as shown in Fig. 2), a maximum error of

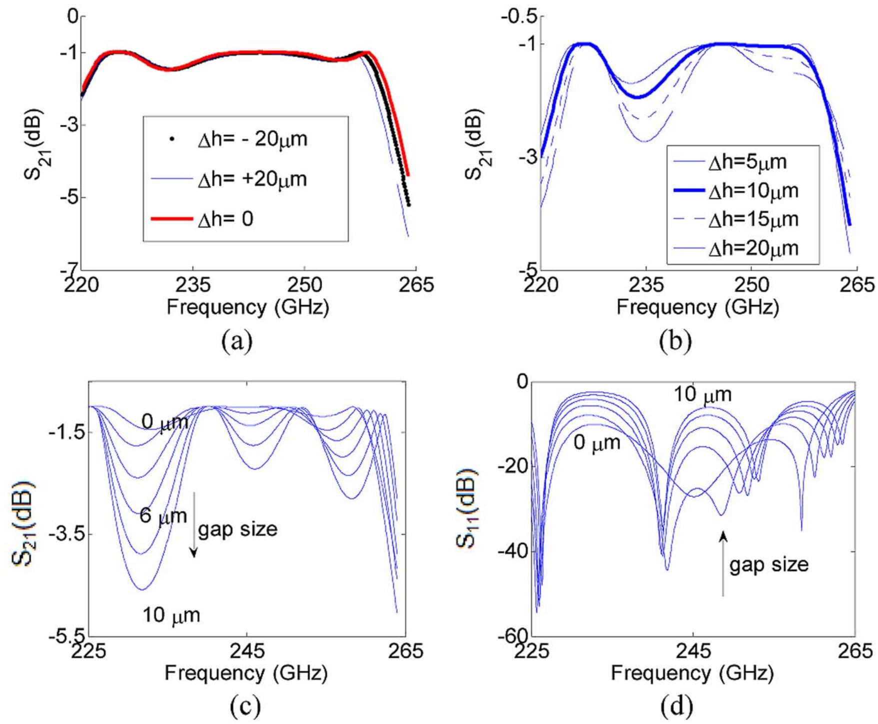

Fig. 11. Transmission coefficient of the transition when (a) h_{WG} is varied $\pm 20\ \mu$m ($\sim$5%) showing the response of the transition is insensitive to variations in waveguide height, b) the response is shown to be more sensitive to the reduced waveguide height h_2 for $\Delta h > 5\ \mu$m. (c) Transmission and (d) reflection coefficients when a gap is modeled between the top of the pin on the bottom wafer and the top wafer. The response degrades for gaps above 3 μm.

about $\pm 20\ \mu$m might be expected for different DRIE runs of depth higher than 400μm. Fig. 11(a) and (b) shows the simulated S-parameters for different values of $h_{\rm WG}$ and h_2. It is shown that errors as high as 20μm (5%) in $h_{\rm WG}$ do not perturb the bandwidth and insertion loss of the transition from its nominal values considerably. For h_2 however, we need to maintain the error within $\pm 5\ \mu$m which is quite achievable. Experimental results on over 10 wafers etched with this method show that the error always remained less than 5 μm deviations.

Mechanical robustness of gold bonding has been verified by dicing and examining the bonded wafers at multiple locations. Visual inspections and mechanical tests trying to separate the segments of bonded wafers all indicated very high quality gold-to-gold bonding. As mentioned before the wafer bonding process had to be done after the top wafer was patterned and etched. One concern here is the lack of pressure over areas where silicon was etched away. One of these critical areas is the point where the shorting pin on the bottom wafer must be connected to the center conductor of the CBCPW line on the top wafer. Fortunately a relatively good electric contact can be established between the pin and the CBCPW center conductors. This is verified by measuring the ohmic resistance between signal and ground. To investigate performance degradation in case of weak gold bonding over the pin, simulations are carried out allowing a small gap between the pin and the center conductor. Fig. 11(c) and (d) represents how much the transmission and reflection coefficients are affected in case the pin is not electrically connected to the top wafer. The results show that the gap size values below 3 μm, does not affect the S-parameters significantly. For the actual structure, since the membrane does not have a considerable amount of stress and does not buckle, a gap larger than a micron is not expected.

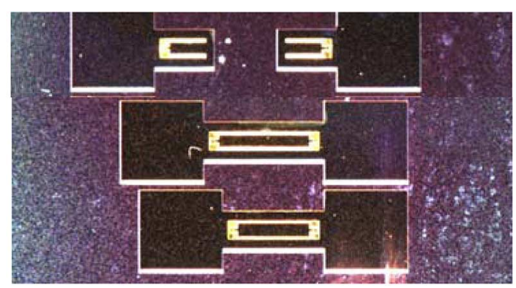

Fig. 12. TRL calibration lines fabricated on the same wafer. Top to bottom: short, line and through.

VI. Measurement Results

In order to de-embed the effect of the grooved CPW line in the measured S-parameters, calibration standards for the designed lines are required. Since it is not feasible to design matched loads for the line, the TRL (through-line-reflect) technique is chosen to calibrate the system. A set of through and half wavelength lines along with a short line is used. These lines include the grooved CPW to CBCPW transition as well and the fabricated set is shown in Fig. 12.

S-parameter measurement of the transition is performed using a dual source PNA-X with OML frequency extenders, as shown in Fig. 13. The structure is fed using GSG probes connected to the frequency extending modules using WR-3 bent

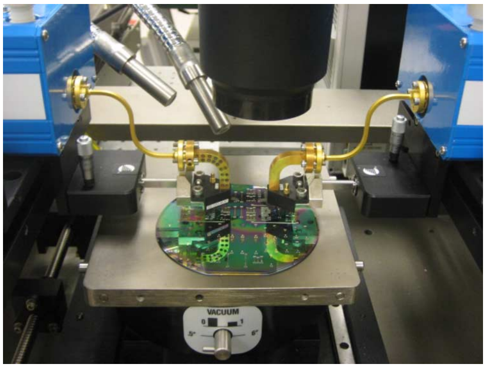

Fig. 13. WR-3 (220–325 GHz) measurement setup. It consists of a dual source PNA-X with OML frequency extenders connected to GSG probes to excite the CPW.

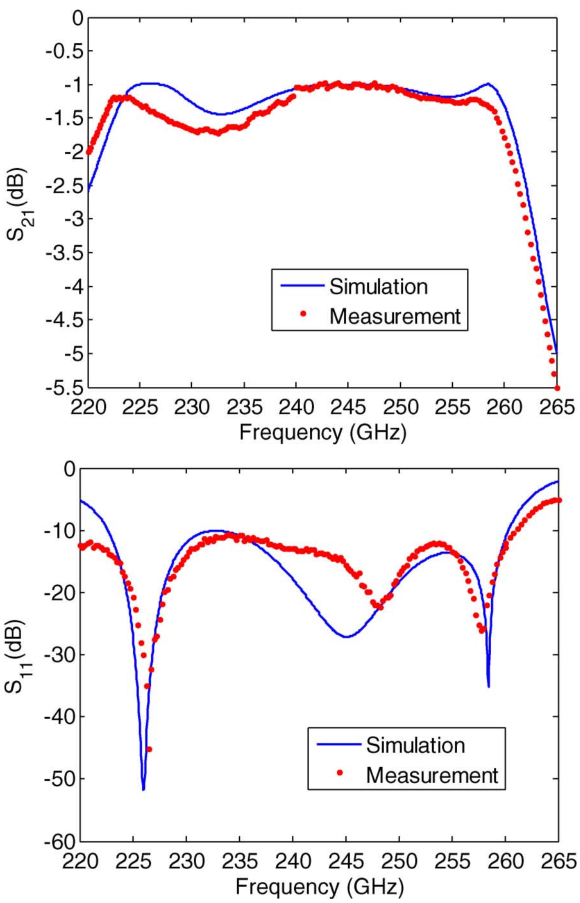

Fig. 14. Measured transmission and reflection coefficients of the back-to-back transition structure of Fig. 2(b). Results are in good agreement with the simulation. Transmission coefficient is below -1.5 dB for the two series transitions and the waveguide section in between.

waveguides controlled by Cascade Microtech MMW micropositioners. On-substrate TRL calibration lines are measured first to de-embed the effect of grooved CPW line. After calibration, S-parameters of the back-to-back transition are measured and presented in Fig. 14. The measurement results show a good agreement with the simulation. Measuring over five different samples on one wafer—which have consistent alignment and thermocompression boding conditions—shows similar minor deviations from the simulation. Therefore, the deviation can be mainly attributed to the error in the probe placement and establishing good contacts on the pads. It should be emphasized that the measured transmission loss includes the loss for the back-to-back transition as well the segment of waveguide in between. The transmission loss associated with one transition is therefore less than 0.6 dB over 220–260 GHz.

VII. Conclusion

A novel transition from cavity-backed CPW to rectangular waveguide using a short-circuited pin in conjunction with resonant sections of CPW and reduced height waveguide segment is presented. The structure is designed to be prismatic (2.5D) with features aligned with the Cartesian coordinate planes to make it compatible with microfabrication processes. A back-to-back structure for standard WR-3 rectangular waveguides was designed with the help of an equivalent circuit model and further analyzed using a full-wave solver. The transition was fabricated using silicon micromachining on two silicon wafers which are bonded together using gold–gold thermocompression bonding technique. The multistep fabrication process and the performance of the transition are evaluated through fabricating a prototype operating at 220–260 GHz. The S-parameters of the structure are measured with a WR-3 network analyzer measurement system and good agreements between measured and simulation results are shown. The microfabrication process is straightforward and the associated tolerances allows for scaling the dimensions and frequency of operation to THz frequencies.

Acknowledgment

The authors would like to thank Dr. J. East, M. Moallem, the staff at the Lurie Nanofabrication Facility (LNF), University of Michigan, Ann Arbor, and the reviewers for their thoughtful comments and suggestions.

References

[1] P. H. Siegel, "Terahertz technology," *IEEE Trans. Microw. Theory Techn.*, vol. 50, no. 3, pp. 910–928, March 2002.

[2] G. E. Ponchak and R. Simons, "A new rectangular waveguide to CPW transition," in *IEEE 1990 MTT-S Int. Microw. Symp. Dig.* , May 1990, vol. 1, pp. 491–492.

[3] C. Dalman, "New waveguide to coplanar waveguide transition for centimetre and millimeter wave application," *Electron. Lett.*, vol. 26, no. 13, pp. 830–831, June 1990.

[4] E. M. Godshalk, "A V-band wafer probe using ridge-through waveguide," *IEEE Trans. Microw. Theory Techn.*, vol. 39, no. 12, pp. 2218–2228, Dec. 1991.

[5] J. de Mingo, A. Moliner, and A. Cameron, "Waveguide-to-coupled fin-line transition in Ka band," *IEEE Microw. Guided Wave Lett.*, vol. 6, no. 19, pp. 363–365, Oct. 1996.

[6] T. Lin and R. Wu, "CPW to waveguide transition with tapered slotline probe," *IEEE Microw. Wireless Compon. Lett.*, vol. 11, pp. 314–316, July 2001.

[7] T. Lin and R. Wu, "A broadband microstrip-to-waveguide transition with tapered CPS probe," in *Proc. 32nd Eur. Microw. Conf.*, Milan, Italy, Sep. 2002, pp. 1–4.

[8] C. Hung *et al.*, "Bandwidth enhancement on waveguide transition to conductor backed CPW with high dielectric constant substrate," *IEEE Microw. Wireless Comp. Lett.*, vol. 15, no. 2, pp. 128–180, Feb. 2005.

[9] A. Ramdane, E. Richalot, O. Picon, J. Puech, and L. Lapierre, "Rectangular waveguide to CPW transition without air-bridge in the Ka-band," *Microw. Opt. Tech. Lett.*, vol. 49, no. 3, pp. 510–513, Jan. 2007.

[10] T. Q. Ho and Y. Shih, "Spectral-domain analysis of E-plane waveguide to microstrip transitions," *IEEE Trans. Microw. Theory Techn.*, vol. 37, no. 2, pp. 388–392, Feb. 1989.

[11] T. Cavanna, J. R. Linkowski, and A. Suriani, "Novel W-band hermetic waveguide-to-coplanar transition," in *3rd ESA Workshop on Millimeter Wave Technol. and Appl.*, Espoo, Finland, May 2003.
[12] T. Cavanna, E. Franzese, E. Limiti, G. Pelosi, S. Selleri, and A. Suriani, "Coplanar-to-rectangular waveguide millimeter-wave transitions manufacturing tolerance analysis," *Int. J. RF and Microw. Computer-Aided Eng.*, vol. 16, pp. 118–124, Mar. 2006.
[13] N. Kaneda, Y. Qian, and T. Itoh, "A broadband CPW-to-waveguide transition using quasi-Yagi antenna," in *Proc. Int. Microw. Symp. Dig.*, Boston, MA, June 2000, vol. 2, pp. 617–620.
[14] R. N. Simons and S. R. Taub, "New coplanar waveguide to rectangular waveguide end launcher," *Electron. Lett.*, vol. 28, no. 12, pp. 1138–1139, Jun. 1992.
[15] J. W. Digby *et al.*, "Fabrication and characterization of micromachined rectangular waveguide components for use at millimeter-wave and terahertz frequencies," *IEEE Trans. Microw. Theory Techn.*, vol. 48, no. 8, pp. 1293–1302, Aug. 2000.
[16] C. E. Collins *et al.*, "A new micro-machined millimeter-wave and terahertz snaptogether rectangular waveguide technology," *IEEE Microw. Guided Wave Lett.*, vol. 9, pp. 63–65, Feb. 1999.
[17] W. R. McGrath, C. Walker, M. Yap, and Y.-C. Tai, "Silion micromachined waveguides for millimeter-wave and submillimeter-wave frequencies," *IEEE Microw. Guided Wave Lett.*, vol. 3, no. 3, pp. 61–63, Mar. 1993.
[18] J. P. Becker, Y. Lee, J. R. East, and L. P. B. Katehi, "A finite ground coplanar line-to-silicon micromachined waveguide transition," *IEEE Trans. Microw. Theory Techn.*, vol. 49, no. 10, p. 2001, Oct. 2001.
[19] Y. Lee, J. P. Becker, J. East, and L. P. B. Katehi, "Fully micromachined finite-ground coplanar line-to-waveguide transitions for w-band applications," *IEEE Trans. Microw. Theory Techn.*, vol. 52, no. 3, pp. 1001–1007, Mar. 2004.
[20] Y. Li, B. Pan, M. M. Tentzeris, and J. Papapolymerou, "A fully micromachined W-band coplanar waveguide to rectangular waveguide transition," in *Proc. 2007 IEEE-IMS Symp.*, Honolulu, HI, Jun. 2007.
[21] Y. Li, B. Pan, C. Lugo, M. M. Tentzeris, and J. Papapolymerou, "Design and characterization of a W-band micromachined cavity filter including a novel integrated transition from CPW feeding lines," *IEEE Trans. Microw. Theory Techn.*, vol. 55, no. 12, pp. 2902–2910, Dec. 2007.
[22] M. Vahidpour and K. Sarabandi, "Ground coplanar waveguide to rectangular waveguide transition," in *Proc. Int. Symp. Antennas Propagat.*, Charleston, NC, 2009.
[23] [Online]. Available: http://www.ggb.com/325.html
[24] N. Marcuvitz, *Waveguide Handbook*. New York: McGraw-Hill, 1951, pp. 271–273.
[25] R. F. Harrington, *Time-Harmonic Electromagnetic Fields*. New York: McGraw-Hill, 1961, pp. 177–179, and 425–428.
[26] R. L. Eisenhart and P. J. Khan, "Theoretical and experimental analysis of a waveguide mounting structure," *IEEE Trans. Microw. Theory Techn.*, vol. 19, no. 8, 1971.
[27] K. Chang and R. L. Ebert, "W-band power combiner design," *IEEE Trans. Microw. Theory Techn.*, vol. 28, no. 4, 1980.
[28] M. Moallem, J. East, and K. Sarabandi, "Optimally designed membrane-supported grounded CPW structure for submillimeter-wave applications," in *Proc. Int. Symp. Antennas Propagat.*, Charleston, NC, 2009.
[29] M. Vahidpour and K. Sarabandi, "Fabrication and performance evaluation of micromachined cavity-backed co-planar waveguide to rectangular waveguide transition at Y-band frequencies," in *Proc. Int. Symp. Antennas Propagat*, Toronto, CA, July 2010.
[30] M. Vahidpour and K. Sarabandi, "Micromachined J-band rectangular waveguide filter," in *Proc. 30th URSI General Assembly and Scientific Symp.*, Istanbul, Turkey, Aug. 2011.
[31] C. H. Tsau, S. M. Spearing, and M. A. Schmidt, "Characterization of wafer-level thermocompression bonds," *J. Microelectromech. Syst.*, vol. 13, pp. 963–971, Dec. 2004.
[32] J. Wu *et al.*, "Study on the gold–gold thermocompression bonding for wafer-level packaging," *Adv. Mater. Res.*, vol. 60–61, pp. 325–329, 2009.

Mehrnoosh Vahidpour (S'99) received the M.Sc. and Ph.D. degrees in electrical engineering from the University of Tehran, Iran, and the University of Michigan at Ann Arbor, in 2005 and 2011, respectively.

She is currently a research scientist at Agilent Technologies. Her research interest includes radar remote sensing, millimeter-wave radars, and microfabrication of high-frequency devices.

Kamal Sarabandi (S'87–M'90–SM'92–F'00) received the B.S. degree in electrical engineering from the Sharif University of Technology, Tehran, Iran, in 1980, the M.S. degree in electrical engineering in 1986, and the M.S. degree in mathematics and the Ph.D. degree in electrical engineering from The University of Michigan at Ann Arbor in 1989.

He is currently the Director of the Radiation Laboratory and the Rufus S. Teesdale Professor of Engineering in the Department of Electrical Engineering and Computer Science, The University of Michigan at Ann Arbor. His research areas of interest include microwave and millimeter-wave radar remote sensing, Meta-materials, electromagnetic wave propagation, and antenna miniaturization. He possesses 25 years of experience with wave propagation in random media, communication channel modeling, microwave sensors, and radar systems and leads a large research group including two research scientists, 12 Ph.D. students. He has graduated 37 Ph.D. and supervised numerous post-doctoral students. He has served as the Principal Investigator on many projects sponsored by the National Aeronautics and Space Administration (NASA), Jet Propulsion Laboratory (JPL), Army Research Office (ARO), Office of Naval Research (ONR), Army Research Laboratory (ARL), National Science Foundation (NSF), Defense Advanced Research Projects Agency (DARPA), and a large number of industries. Currently he is leading the Center for Microelectronics and Sensors funded by the Army Research Laboratory under the Micro-Autonomous Systems and Technology (MAST) Collaborative Technology Alliance (CTA) program. He has published many book chapters and more than 190 papers in refereed journals on miniaturized and onchip antennas, meta-materials, electromagnetic scattering, wireless channel modeling, random media modeling, microwave measurement techniques, radar calibration, inverse scattering problems, and microwave sensors. He has also had more than 442 papers and invited presentations in many national and international conferences and symposia on similar subjects.

Dr. Sarabandi served as a member of NASA Advisory Council appointed by the NASA Administrator for two consecutive terms from 2006–2010. He is serving as a vice president of the IEEE Geoscience and Remote Sensing Society (GRSS) and is a member of the Editorial Board of the PROCEEDINGS OF THE IEEE. He was an associate editor of the IEEE TRANSACTIONS ON ANTENNAS AND PROPAGATION and the IEEE SENSORS JOURNAL. He is a member of Commissions F and D of URSI. Dr. Sarabandi was the recipient of the Henry Russel Award from the Regent of The University of Michigan. In 1999 he received a GAAC Distinguished Lecturer Award from the German Federal Ministry for Education, Science, and Technology. He was also a recipient of the 1996 EECS Department Teaching Excellence Award and a 2004 College of Engineering Research Excellence Award. In 2005 he received the IEEE GRSS Distinguished Achievement Award and the University of Michigan Faculty Recognition Award. He also received the best paper Award at the 2006 Army Science Conference. In 2008 he was awarded a Humboldt Research Award from The Alexander von Humboldt Foundation of Germany and received the best paper award at the IEEE Geoscience and Remote Sensing Symposium. He was also awarded the 2010 Distinguished Faculty Achievement Award from the University of Michigan. The IEEE Board of Directors announced him as the recipient of the 2011 IEEE Judith A. Resnik medal. In the past several years, joint papers presented by his students at a number of international symposia (IEEE APS'95,'97,'00,'01,'03,'05,'06,'07; IEEE IGARSS'99,'02,'07;'11 IEEE IMS'01, USNC URSI'04,'05,'06,'10,'11 AMTA '06, URSI GA 2008) have received best paper awards.